applied sciences

MDPI

Article

An Unsupervised Method of Change Detection in Multi-Temporal PolSAR Data Using a Test Statistic and an Improved K&I Algorithm

Jinqi Zhao [1,2], Jie Yang [1,*], Zhong Lu [2], Pingxiang Li [1], Wensong Liu [1] and Le Yang [1]

[1] State Key Laboratory of Information Engineering in Surveying, Mapping and Remote Sensing, Wuhan University, Wuhan 430079, China; masurq@whu.edu.cn (J.Z.); pxli@whu.edu.cn (P.L.); liuwensongupc@163.com (W.L.); yangleupc@163.com (L.Y.)

[2] Huffington Department of Earth Sciences, Southern Methodist University, Dallas, TX 75275, USA; zhonglu@smu.edu

* Correspondence: yangj@whu.edu.cn; Tel.: +86-139-7151-2278

Received: 30 October 2017; Accepted: 8 December 2017; Published: 13 December 2017

Abstract: In recent years, multi-temporal imagery from spaceborne sensors has provided a fast and practical means for surveying and assessing changes in terrain surfaces. Owing to the all-weather imaging capability, polarimetric synthetic aperture radar (PolSAR) has become a key tool for change detection. Change detection methods include both unsupervised and supervised methods. Supervised change detection, which needs some human intervention, is generally ineffective and impractical. Due to this limitation, unsupervised methods are widely used in change detection. The traditional unsupervised methods only use a part of the polarization information, and the required thresholding algorithms are independent of the multi-temporal data, which results in the change detection map being ineffective and inaccurate. To solve these problems, a novel method of change detection using a test statistic based on the likelihood ratio test and the improved Kittler and Illingworth (K&I) minimum-error thresholding algorithm is introduced in this paper. The test statistic is used to generate the comparison image (CI) of the multi-temporal PolSAR images, and improved K&I using a generalized Gaussian model simulates the distribution of the CI. As a result of these advantages, we can obtain the change detection map using an optimum threshold. The efficiency of the proposed method is demonstrated by the use of multi-temporal PolSAR images acquired by RADARSAT-2 over Wuhan, China. The experimental results show that the proposed method is effective and highly accurate.

Keywords: change detection; test statistic; improved Kittler and Illingworth (K&I); generalized Gaussian model (GGM); PolSAR; multi-temporal

1. Introduction

Change detection is the process of identifying the differences on the Earth's surface by multi-temporal images acquired in the same geographical area at different times [1,2]. During recent years, because of the advantage of repetitive data acquisition, both satellite images and aerial photographs obtained by optical and synthetic aperture radar (SAR) sensors have been widely used in land-cover change detection. The change information is important because of its practical use in applications such as land-use and land-cover dynamic analysis [3,4] and environmental monitoring [5,6].

Although optical images have been widely applied in change detection [2,3,7], night-time and severe weather limit the use of optical images in practice. Because SAR is an active microwave sensor with all-weather, day-and-night operational imaging capability [8], the use of SAR sensors instead of optical sensors is attractive in change detection studies [9]. Recently, many researchers have focused

on change detection and time-series analysis based on SAR images [10–12]. Several methods have been designed for single-channel SAR images [13–16], but the interpretation of the backscattering changes in land cover is limited [6]. Compared with single-channel SAR images, polarimetric SAR (PolSAR) sensors acquire phase and amplitude information in different polarizations, and thus offer more scattering information [17,18]. However, literature on change detection with PolSAR data is sparse [9]. Because of the potential to provide improved detection capability and to extend the application of PolSAR data in change detection, we explore multi-temporal PolSAR data for change detection in this study.

Change detection based on multi-temporal PolSAR images can be classified into two categories: supervised and unsupervised [19]. Although the supervised method, such as the widely used post-classification comparison (PCC), can provide more information on both the change extent and the type of change [18], it can be easily biased by the cumulative error caused by the classification of individual remote sensing image during change detection processing. Moreover, the supervised change detection technique depends on the classification accuracy of multi-temporal PolSAR imagery, which can be easily affected by manual intervention (such as the training sample selection). Compared with the supervised method, the unsupervised change detection approach is relatively straightforward, easy to implement and interpret without human intervention. Due to these reasons, this paper focuses on change detection based on an unsupervised method.

In general, unsupervised change detection in SAR images includes three steps: (1) preprocessing, (2) generating the comparison image (CI), and (3) making a decision based on the analysis of the CI in order to obtain the binary change map [9,18]. The preprocessing of multi-temporal SAR images is a critical step in the change detection and involves radiometric calibration, image co-registration, and speckle filtering. Radiometric calibration is necessary for the comparison of SAR images acquired at different dates. After radiometric calibration, the pixel values of multi-temporal SAR images are related to the radar backscattering. Image co-registration [20,21] is aimed at reducing the errors caused by the misregistration of the images and aligns the images used in the change detection as precisely as possible. Speckle noise needs to be suppressed by speckle filtering [22] before change detection. In order to obtain a good result in unsupervised change detection, the second and third steps play an important role in processing.

The change detection result depends on both the quality of the CI (Step 2) and the quality of the threshold choice (Step 3) [11,14]. In order to obtain the CI in the second step, there are many different approaches that can be used to compare the preprocessed images of the same geographical area at different dates. These methods can be divided into two main categories: (1) methods based on pixel radiometry and (2) methods based on local statistics [23]. Each of these two categories has its own advantages and disadvantages. The approaches based on pixel radiometry are widely used and easy to design in multi-temporal SAR images, but they are easily influenced by speckle noise. The approaches based on local statistics combine the homogeneous pixels together, which effectively reduces the influence of speckle [24–26], but they do require many prior parameters. As a result, none of these methods can be regarded as optimal, and there is also no common standard at present [11]. In this paper, we focus on change detection based on pixel radiometry. The methods based on pixel radiometry are widely used with multi-temporal SAR images. Such methods include the ratio or log-ratio operator of SAR amplitudes or intensities [13,15,16], change vector analysis (CVA) [27], principal component analysis (PCA) [28,29], the hidden Markov chain model [30,31], and the Kullback–Leibler divergence method [32]. These methods are usually applied in multi-temporal single-channel SAR-based change detection. When a test statistic [5] was first used in change detection, it was assumed that the covariance (or coherency) matrices follow a complex Wishart distribution, but only the azimuthally symmetric case and the diagonal-element-only case were used to detect the changes. The method proposed in [4] uses all the elements of the covariance (or coherency) matrices to obtain the change detection map. In the third step of change detection analysis, the change detection map can be obtained by the decision threshold of the CI. Several algorithms have been widely used to automatically determine

the threshold, such as the constant false alarm rate (CFAR) algorithm [33,34], Otsu's thresholding method [35], Kapur's entropy algorithm [36], and the Kittler and Illingworth (K&I) algorithm [37].

In this paper, we assume a complex Wishart distribution for the coherency matrix and apply a test statistic based on maximum likelihood estimation (MLE) and an improved K&I algorithm based on a generalized Gaussian model (GGM). The test statistic using more scattering information from the multi-temporal PolSAR images can obtain a high-precision CI. Moreover, the probability density function (PDF) of the CI can be simulated by the GGM. Because the traditional K&I algorithm using the Gaussian model to select the threshold automatically is not fit for CI from PolSAR data at different dates, we apply the GGM to the K&I algorithm to choose the threshold. After finishing the procedure, we can obtain the binary change detection map (changed and unchanged).

The remainder of this paper is organized as follows. Section 2 presents a brief introduction to the fundamental theory and details of the proposed change detection framework. Section 3 describes the experimental results. In Section 4, we draw our conclusion.

2. Materials and Methods

2.1. The Model of PolSAR Data

Assuming that a p-dimensional random complex vector $K = [k_1, k_2, \ldots, k_p]^T$ follows a complex multivariate normal distribution with mean 0 and dispersion matrix $\Sigma_K = E\left[\left\langle KK^{*T}\right\rangle\right]$, the $p \times p$ matrix Σ is a Hermitian positive definite random matrix and follows a Wishart distribution. A PolSAR system measures the amplitude and phase of the backscattered signals in four combinations of linear receive and transmit polarizations: horizontal–horizontal (hh), horizontal–vertical (hv), vertical–horizontal (vh), and vertical–vertical (vv) [5,26]. Assuming that the target reciprocity condition is satisfied [22], the polarimetric information can be expressed by a complex vector:

$$\Omega = \left[S_{hh}, \sqrt{2}S_{hv}, S_{vv}\right]^T \tag{1}$$

where h and v denote the horizontal and vertical wave polarization states, T indicates the vector transposition, and S_{hv} is the scattering element of the horizontal transmitting and vertical receiving polarizations.

For multi-look processed PolSAR data, the backscattered signal can be expressed as a covariance matrix:

$$C = \left\langle \Omega \cdot \Omega^{*T} \right\rangle = \left\langle \begin{bmatrix} |S_{hh}|^2 & S_{hh}S_{hv}^* & S_{hh}S_{vv}^* \\ S_{hv}S_{hh}^* & |S_{hv}|^2 & S_{hv}S_{vv}^* \\ S_{vv}S_{hh}^* & S_{vv}S_{hv}^* & |S_{vv}|^2 \end{bmatrix} \right\rangle \tag{2}$$

The covariance matrix C can be modeled by a complex Wishart distribution. The frequency function of covariance matrix C can be shown as follows:

$$\begin{gathered} f(C) = \frac{1}{\Gamma_p(n)} \frac{1}{|\Sigma_\Omega|^n} |C|^{n-p} \exp\left\{-tr[\Sigma_\Omega^{-1}C]\right\} \\ \Gamma_p(n) = \pi^{p(p-1)/2} \prod_{j=1}^{p} \Gamma(n-j+1) \end{gathered} \tag{3}$$

where $tr(\cdot)$ is the trace operator, n is the number of looks, $\Gamma_p(n)$ is a normalization factor, and $\Sigma_\Omega = E\left[\left\langle \Omega \cdot \Omega^{*T} \right\rangle\right]$.

2.2. The Proposed Method

Test Statistic for the Equality of Two Covariance Matrices

We consider that the two covariance matrices (C_1,C_2) from the bi-temporal PolSAR images are independent and follow a Wishart distribution as follows:

$$\begin{array}{c} C_1 \in W(p, m, \Sigma_{C_1}) \\ C_2 \in W(p, n, \Sigma_{C_2}) \end{array} \tag{4}$$

where p represents the dimensions of C_1 and C_2, and m and n represent the number of looks of C_1 and C_2, respectively. Σ_{C_1} and Σ_{C_2} represent the dispersion matrix of C_1 and C_2, and the MLE of Σ_{C_1} and Σ_{C_2} can be shown as follows:

$$\Sigma_{C_1}^{MLE} = \frac{1}{m} C_1 \text{ and } \Sigma_{C_2}^{MLE} = \frac{1}{n} C_2. \tag{5}$$

Assuming that the null hypothesis $H_0 : \sum_{C_1} = \sum_{C_2}$ means that the two matrices are equal and there is a strong possibility of non-change, the alternative hypothesis $H_1 : \sum_{C_1} \neq \sum_{C_2}$ means that the two matrices are different and there is a strong possibility of change [5].

We suppose that the test statistics based on MLE have joint densities $f(\sum_{C_1}, \sum_{C_2}, \theta)$, where θ is the set of parameters of the probability function that has generated the data. Then H_0 states that $\theta \in H_0$, and the likelihood ratio of the test statistic is shown as follows [5]:

$$Q = \frac{\max_{\theta \in H_0} L(\theta)}{\max_{\theta \in \Omega} L(\theta)} \text{ where } L(\theta) = f(\sum_{C_1}, \sum_{C_2}, \theta) = f(\sum_{C_1}, \theta) f(\sum_{C_2}, \theta) \tag{6}$$

where $\Omega = H_0 \cup H_1$, $L(\cdot)$ is the likelihood function, and $f(\cdot)$ is the frequency function.

Putting Equation (3) into Equation (6) and assuming $\Sigma_{C_1} = \Sigma_{C_2} = \Sigma$, $L(\theta)$ can be expressed as follows [5]:

$$L(\theta) = \frac{1}{\Gamma_p(n)\Gamma_p(m)} |\Sigma|^{-n-m} |C_1|^{n-p} |C_2|^{m-p} \exp\{-tr[\Sigma^{-1}(C_1 + C_2)]\} \in W_C(p, n+m, \Sigma) \tag{7}$$

The MLE of Equation (6) can be simplified as follows [5]:

$$Q = \frac{L(\overline{\Sigma})}{L_{C_1}(\overline{\Sigma}_{C_1}) L_{C_2}(\overline{\Sigma}_{C_2})} = \frac{(n+m)^{p(n+m)}}{n^{pn} m^{pm}} \frac{|C_1|_n |C_2|^m}{|C_1 + C_2|^{n+m}} \tag{8}$$

Assuming $m = n$, the CI of the bi-temporal PolSAR images can be denoted by d:

$$d = -2\rho ln Q = -2\rho n(2pln2 + ln|C_1| + ln|C_2| - ln|C_1 + C_2|) \tag{9}$$

where ρ can be represented as follows:

$$\rho = 1 - \frac{2p^2 - 1}{6p} \left(\frac{1}{n} + \frac{1}{m} - \frac{1}{n+m}\right). \tag{10}$$

2.3. Improved K&I

After obtaining the CI of the bi-temporal PolSAR data, an automatic method of threshold selection is introduced. The K&I algorithm for the automatic estimation of the optimal threshold is suitable for SAR data [4,14,15,26] and has been widely used to distinguish the changed and unchanged classes in the CI. The K&I thresholding method is an extension of Bayes' minimum-error probability theory and can be shown as follows:

$$J(T) = \sum_{d_l=0}^{L-1} h(d_l) c(d_l, T) \text{ where } c(d_l, T) = \begin{cases} -2 \ln P(\omega_u | d_l, T), d_l \leq T \\ -2 \ln P(\omega_c | d_l, T), d_l > T \end{cases} \tag{11}$$

where $h(d_l)$ and L represent the histogram and the number of possible gray levels of the CI, respectively, and $c(d_l, T)$ denotes the cost of classifying pixels by comparing the corresponding gray level d_l

and threshold T. $P(\omega_i|d_l, T)$ $(i = u, c)$ is the posterior probability, which represents the unchanged (or changed) class under the condition of gray level d_l and a specific value of the threshold T.

The optimal threshold corresponding to minimizing the classification error is the following cost function [37]:

$$T^* = \arg \min_{T=0,1,\ldots,L-1} J(T) \tag{12}$$

Using Bayes' theorem, the posterior probability can be expressed by the prior probability and class-conditional PDF, i.e.,

$$P(\omega_i|d_l, T) = \frac{P(\omega_i) \cdot P(d_l|\omega_i, T)}{\sum_{j\in\{u,c\}} P(\omega_j) \cdot P(d_l|\omega_j, T)}. \tag{13}$$

The traditional K&I method assumes that the class-conditional distribution follows a Gaussian distribution, but this assumption cannot accurately reflect the distribution of the CI. In order to improve the threshold selection, an improved model based on the GGM describing the statistical behaviors of the changed and unchanged classes in the CI can be used. The model of the class-conditional PDF is shown as follows [14]:

$$P(d_l|\omega_i, T) = a_i(T)e^{-[b_i(T)|d_l - m_i(T)|]^{\beta_i(T)}}, i = u, c \text{ where } a_i(T) = \frac{b_i(T)\beta_i(T)}{2\Gamma(1/\beta_i(T))}, b_i(T) = \frac{1}{\sigma_i(T)}\sqrt{\frac{\Gamma(3/\beta_i(T))}{\Gamma(1/\beta_i(T))}} \tag{14}$$

where terms $m_i(T)$, $\sigma_i(T)$, and $\beta_i(i = u, c)$ are the means, the variances, and the shape parameters of the distribution based on the unchanged and changed classes, respectively. Different values of shape parameters can generate different styles of density function [38]. In the proposed method, we choose the GGM to estimate the class-conditional PDF, and the criterion $J(T)$ can be expressed as follows [14]:

$$\begin{aligned} J(T) = &\sum_{d_l=0}^{T} h(d_l)\left[b_u(T)|d_l - m_u(T)|\right]^{\beta_u(T)}] + \sum_{d_l=T+1}^{L-1} h(d_l)\left[b_c(T)|d_l - m_c(T)|\right]^{\beta_c(T)}] \\ &-[p_u(T)\log p_u(T) + P_c(T)\log P_c(T)] - [P_u(T)\log a_u(T) + P_c(T)\log a_c(T)] \end{aligned} \tag{15}$$

Associated with the unchanged and changed classes, $p_u(T)$ and $p_c(T)$ denote the prior probabilities, $m_u(T)$ and $m_c(T)$ denote the means, and $\sigma_u(T)$ and $\sigma_c(T)$ denote the variances. These parameters of the above formula are estimated by the gray level d_l and the histogram $h(d_l)$ in Equation (16):

$$\begin{cases} P_u(T) = \sum_{d_l=0}^{T} h(d_l) \\ m_u(T) = \frac{1}{P_u(T)} \sum_{d_l=0}^{T} d_l h(d_l) \\ \sigma_u^2(T) = \frac{1}{P_u(T)} \sum_{d_l=0}^{T} [d_l - m_u(T)]^2 h(d_l) \\ E[|d_l||\omega_u] = \frac{1}{P_u(T)} \sum_{d_l=0}^{T} h(d_l)|d_l - m_u(T)| \\ P_c(T) = 1 - P_u(T) \\ m_c(T) = \frac{1}{P_c(T)} \sum_{d_l=T+1}^{L-1} d_l h(d_l) \\ \sigma_c^2(T) = \frac{1}{P_c(T)} \sum_{d_l=T+1}^{L-1} [d_l - m_c(T)]^2 h(d_l) \\ E[|d_l||\omega_c] = \frac{1}{P_i(T)} \sum_{d_l=T+1}^{L-1} h(d_l)|d_l - m_u(T)| \\ r(\beta_i) = \frac{\Gamma(1/\beta_i)\Gamma(3/\beta_i)}{\Gamma^2(2/\beta_i)} \\ \chi_i = \frac{\sigma_i^2}{E^2[|d_l||\omega_i]} \\ \beta_i = r^{-1}(\chi_i) \end{cases}. \tag{16}$$

2.4. The Proposed Method

The entire procedure of the proposed method is as follows:

Step (1): The bi-temporal PolSAR images need to be co-registered and filtered. Image registration is performed to align the images used in the change detection. Speckle filtering is commonly used to suppress speckle noise before the change detection and classification of PolSAR images. The preprocessing is important for change detection. In this study, the refined Lee filter [39] was used to remove the speckle noise.

Step (2): The CI is obtained by the test statistic using the covariance matrices of the bi-temporal images. In this step, bi-temporal fully PolSAR data are used to generate the CI.

Step (3): The improved K&I algorithm based on the GGM is used to simulate the distribution of the CI and obtain the optimum threshold for the CI.

Step (4): The unchanged and changed classes of position (i, j) are determined. If $d_{ij} < T$, this means that the PolSAR data in the same position at different dates are similar; otherwise, the corresponding pixel positions are different. Finally, the change detection map is obtained.

The detailed processing flow of the proposed method is shown in Figure 1.

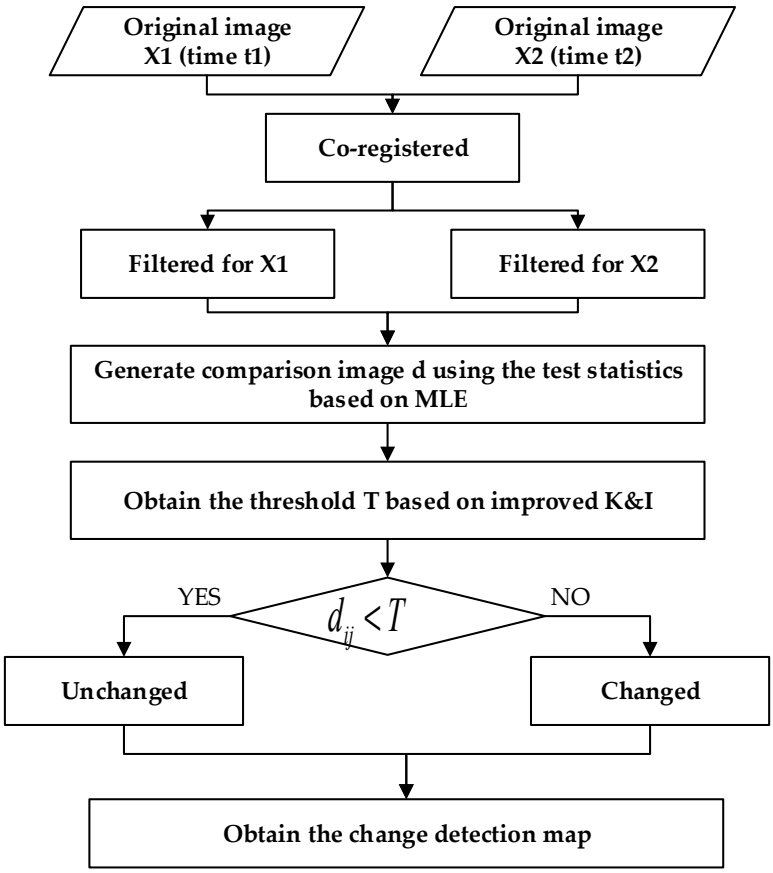

Figure 1. The flowchart of the proposed method.

2.5. Evaluation Criterion

Quantitative evaluation is important to determine the result of the change detection. When the ground truth is available, a quantitative evaluation can be performed [18,40]. We used the false alarm (FA) rate, the total errors (TEs), the overall accuracy (OA), and the Kappa coefficient [41] to verify the accuracy of the results based on the proposed method. These indicators are calculated as follows:

$$\begin{cases} FA = \frac{FP}{N_u} \\ N = N_u + N_c \\ TE = \frac{FP+FN}{N}, OA = \frac{TP+TN}{N} \\ Kappa = \frac{OA-Pe}{1-Pe} \\ Pe = \frac{(TP+FN)(TP+FP)+(FP+TN)(FN+TN)}{N^2} \end{cases} \quad (17)$$

where TP (true positives) means the number of changed points correctly detected; TN (true negatives) means the number of unchanged points correctly detected; FP (false positives) means the number of unchanged points incorrectly detected as changed (false alarms); FN (false negatives) means the number of changed points incorrectly detected as unchanged (missed detections). N_u and N_c are the number of unchanged points and changed points of the ground reference change map, respectively.

3. Results and Discussion

3.1. Study Area and Background

The city of Wuhan (Figure 2) is situated in the east of Hubei province, China and lies in the eastern Jianghan Plain, at the intersection of the middle reaches of the Yangtze River. Its climate is humid subtropical, with abundant rainfall and four distinct seasons. From 2011 to 2016, the construction of a new tunnel and its ancillary buildings took place on East Lake. After the new tunnel was completed, the ancillary buildings were removed in 2016. Moreover, in July 2016, a 50-year return period of rainfall occurred, and the rainfall was significantly higher than the average annual precipitation. Wuhan was affected by continuous heavy rain, and some areas were seriously flooded and dramatically changed. The use of optical sensors was limited by this severe weather. In this study, our aim was to monitor the changes associated with the tunnel construction on East Lake from three temporal PolSAR images (2011, 2015, and 2016) and to use bi-temporal PolSAR images (2015 and 2016) to detect the changes after the heavy rainfall.

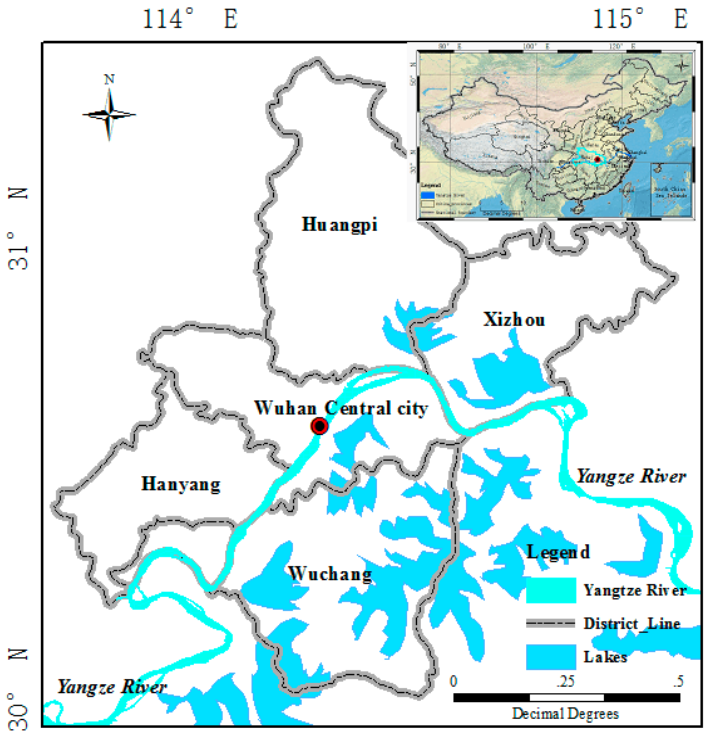

Figure 2. Location of the study area.

Three C-band quad-polarimetric RADARSAT-2 (single look complex) images of Wuhan were acquired on 7 December 2011, 25 June 2015, and 6 July 2016. The nominal pixel spacings in the azimuth and range directions were 5.12 × 4.73 m (7 December 2011 and 25 June 2015) and 4.86 × 4.73 m (6 July 2016). The swath width was 25 × 25 km, and the beams of the images were FQ21 (7 December 2011 and 25 June 2015) and FQ27 (6 July 2016), with the incidence angle ranging from 40.16° to 41.58° (7 December 2011 and 25 June 2015) and 45.23° to 46.49° (6 July 2016). The repeat cycle was 24 days. The preprocessing of temporal PolSAR data is important for change detection. In this study, the preprocessing consisted of radiometric calibration, speckle filtering, and image co-registration. After the radiometric calibration, the pixel values of the temporal PolSAR images are directly related to the radar backscatter of the scene. This condition is necessary for the comparison of PolSAR images acquired at different dates. Speckle filtering and image co-registration were also performed. Two free open-source software packages—the Next ESA SAR Toolbox and the PolSARpro SAR Data Processing and Educational Tool—were used in the preprocessing of the SAR datasets. The co-registered images of 2011 and 2015 were of 5058 × 5696 pixels, and the co-registered images of 2015 and 2016 were of 4906 × 5114 pixels.

The Pauli-RGB images ($|S_{hh} - S_{vv}|$ for red, $|S_{hv}|$ for green, and $|S_{hh} + S_{vv}|$ for blue) are shown in Figure 3a–c. Due to the large study areas, long intervals (2011–2015), and inclement weather conditions (heavy rainfall in July 2016), the regions labeled by the three red boxes are used to give a detailed assessment, to verify the efficiency of the proposed method. These labeled regions involve bridge, city, forest, and water bodies. Region 1 is East Lake, Region 2 is Yanxi Lake, and Region 3 is Yandong Lake. The ground reference maps over the three test sites were obtained based on the corresponding optical images obtained from Google Earth (version 7.18) and field surveys conducted by researchers.

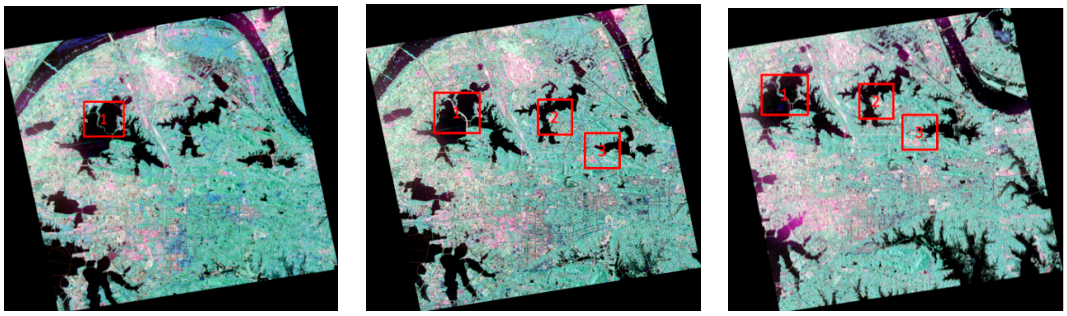

(**a**) (**b**) (**c**)

Figure 3. RADARSAT-2 PolSAR images acquired on (**a**) 7 December 2011, (**b**) 25 June 2015, and (**c**) 6 July 2016.

3.1.1. Change Detection Based on the Images from 2011, 2015, and 2016

The images from the three different dates display the changes associated with the construction of the new tunnel on East Lake. In order to give a detailed assessment, we separated the dataset into two groups. The first group was made up of the data from 2011 and 2015, and the second group was made up of the data from 2015 and 2016. To verify the efficiency of the proposed method, comparative experiments were designed. We compared change detection methods based on log-ratio (HH) and improved K&I, log-ratio (HV) and improved K&I, log-ratio (VV) and improved K&I, CVA and improved K&I, a test statistic with a 5% significance level, a test statistic with a 1% significance level, a test statistic and K&I, a test statistic and CFAR, and a test statistic and improved K&I (the proposed method). The results of the change detection for the first and second groups of images are shown in Figures 4 and 5, respectively.

The highlighted box labeled as Region 1 is used to give a detailed assessment. The land-cover types of this area are lake, bridge, city, and forest. The size of this area is 800 × 500 pixels, and the Pauli-RGB images are shown in Figure 6a–c.

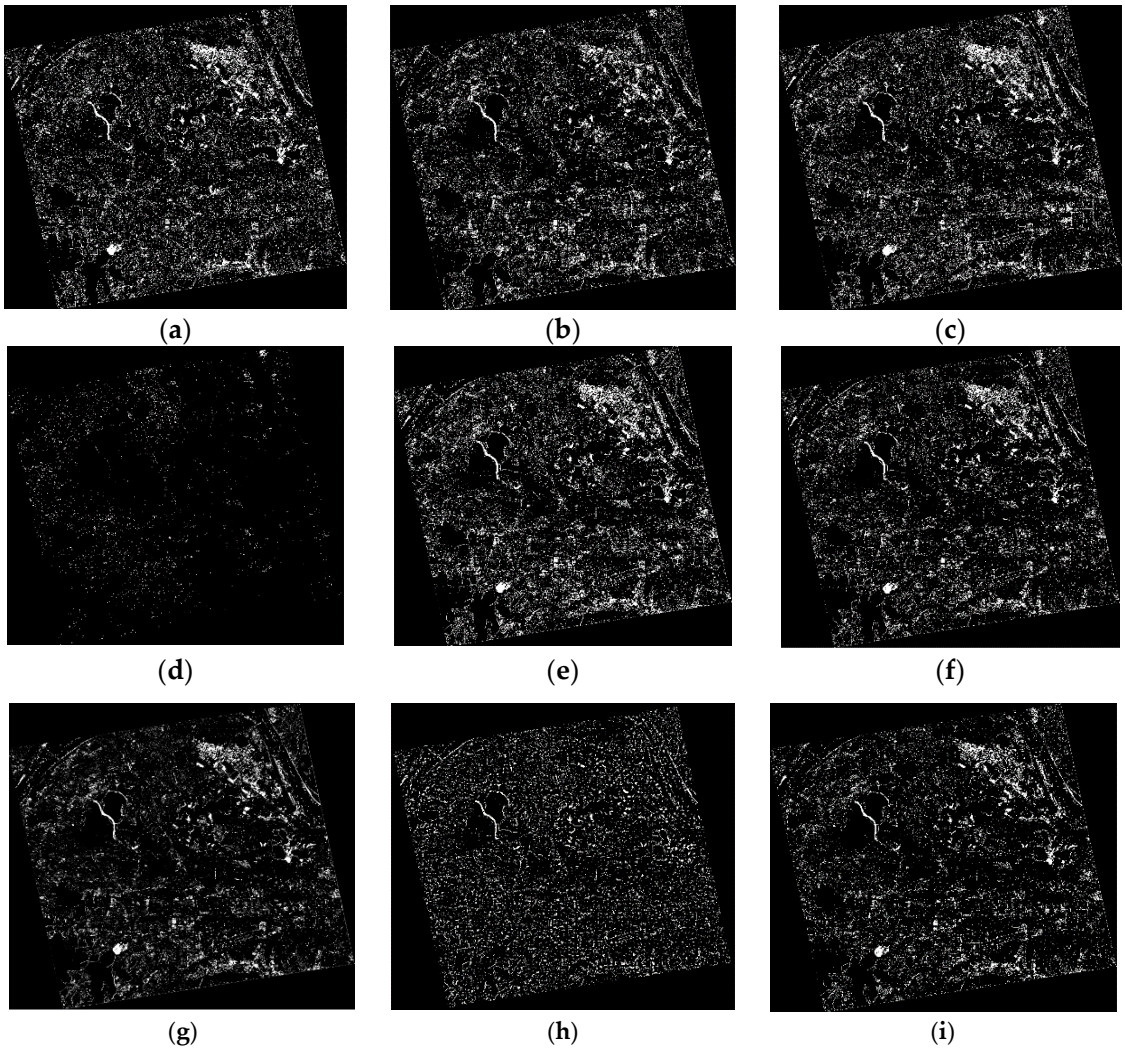

Figure 4. Change detection maps of full frame between 2011 and 2015 based on the following: (**a**) log-ratio (HH) and improved K&I; (**b**) log-ratio (HV) and improved K&I; (**c**) log-ratio (VV) and improved K&I; (**d**) CVA and improved K&I; (**e**) test statistic with 5% significance level; (**f**) test statistic with 1% significance level; (**g**) test statistic and K&I; (**h**) test statistic and CFAR; (**i**) test statistic and improved K&I (the proposed method).

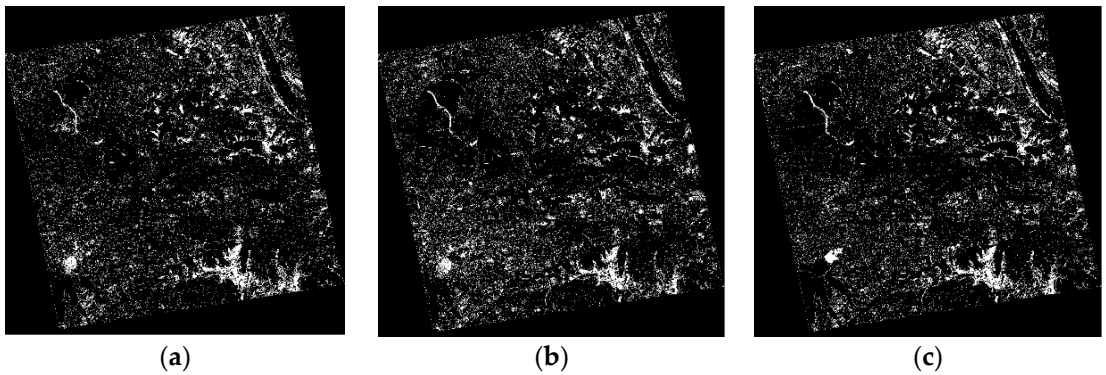

Figure 5. *Cont*.

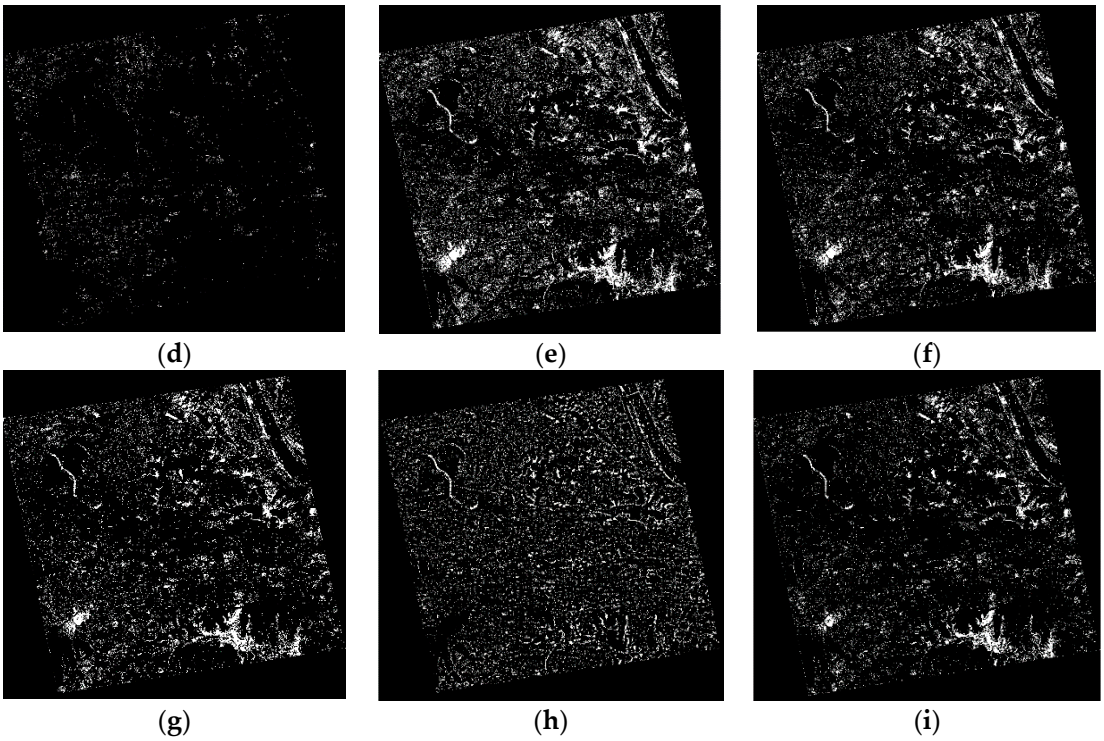

Figure 5. Change detection maps of full frame between 2015 and 2016 based on the following: (**a**) log-ratio (HH) and improved K&I; (**b**) log-ratio (HV) and improved K&I; (**c**) log-ratio (VV) and improved K&I; (**d**) CVA and improved K&I; (**e**) test statistic with 5% significance level; (**f**) test statistic with 1% significance level; (**g**) test statistic and K&I; (**h**) test Statistic and CFAR; (**i**) test statistic and improved K&I (the proposed method).

Figure 6. RADARSAT-2 PolSAR images of Region 1 indicated in Figure 3, acquired on (**a**) 7 December 2011, (**b**) 25 June 2015, and (**c**) 6 July 2016.

The results of the CI maps and their 3-D plots are shown by linear mapping to [0, 1] in Figures 7 and 8, respectively. Although the CI maps of the log-ratio (HH) method (Figures 7a and 8a) show a strong response in the changed area, the contrast between the changed and unchanged areas is not obvious. Moreover, there is also a high response in the unchanged area because of the speckle noise, which impacts the accuracy of the change detection map. The CI maps of the CVA method (Figures 7b and 8b) show a weak response, which makes it difficult to distinguish the changed and

unchanged areas. The proposed method (Figures 7c and 8c) using the fully polarimetric information also shows a strong response in the changed areas (the bridge and the edges of the water bodies). However, unlike the other methods, the proposed method shows a low response in the water bodies. Overall, the proposed method of generating the CI map is able to accurately distinguish the changed and unchanged areas.

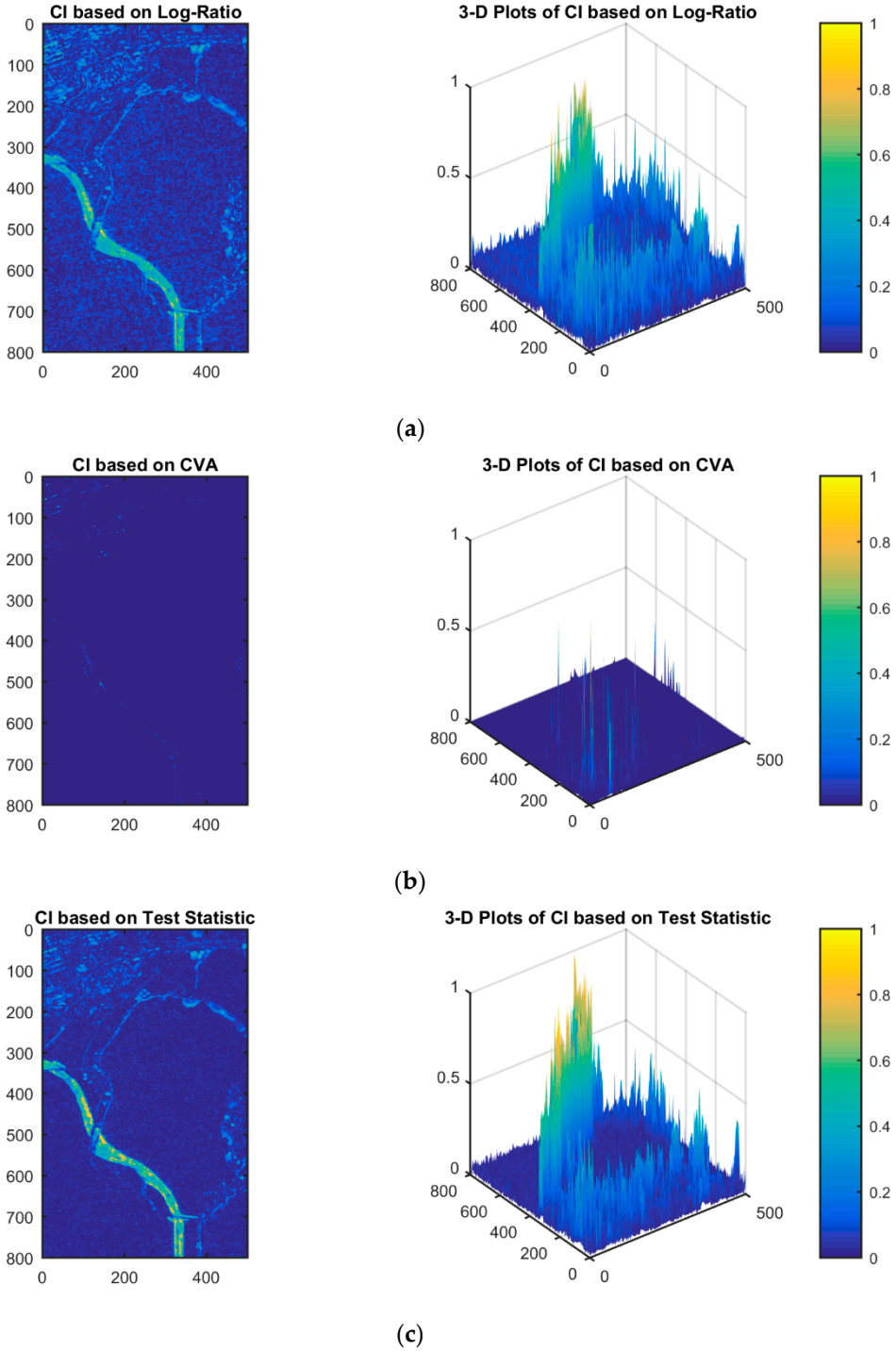

Figure 7. CI maps and 3-D plots of Region 1 based on (**a**) log-ratio (HH), (**b**) CVA, and (**c**) test statistics for the different dates of 7 December 2011 and 25 June 2015.

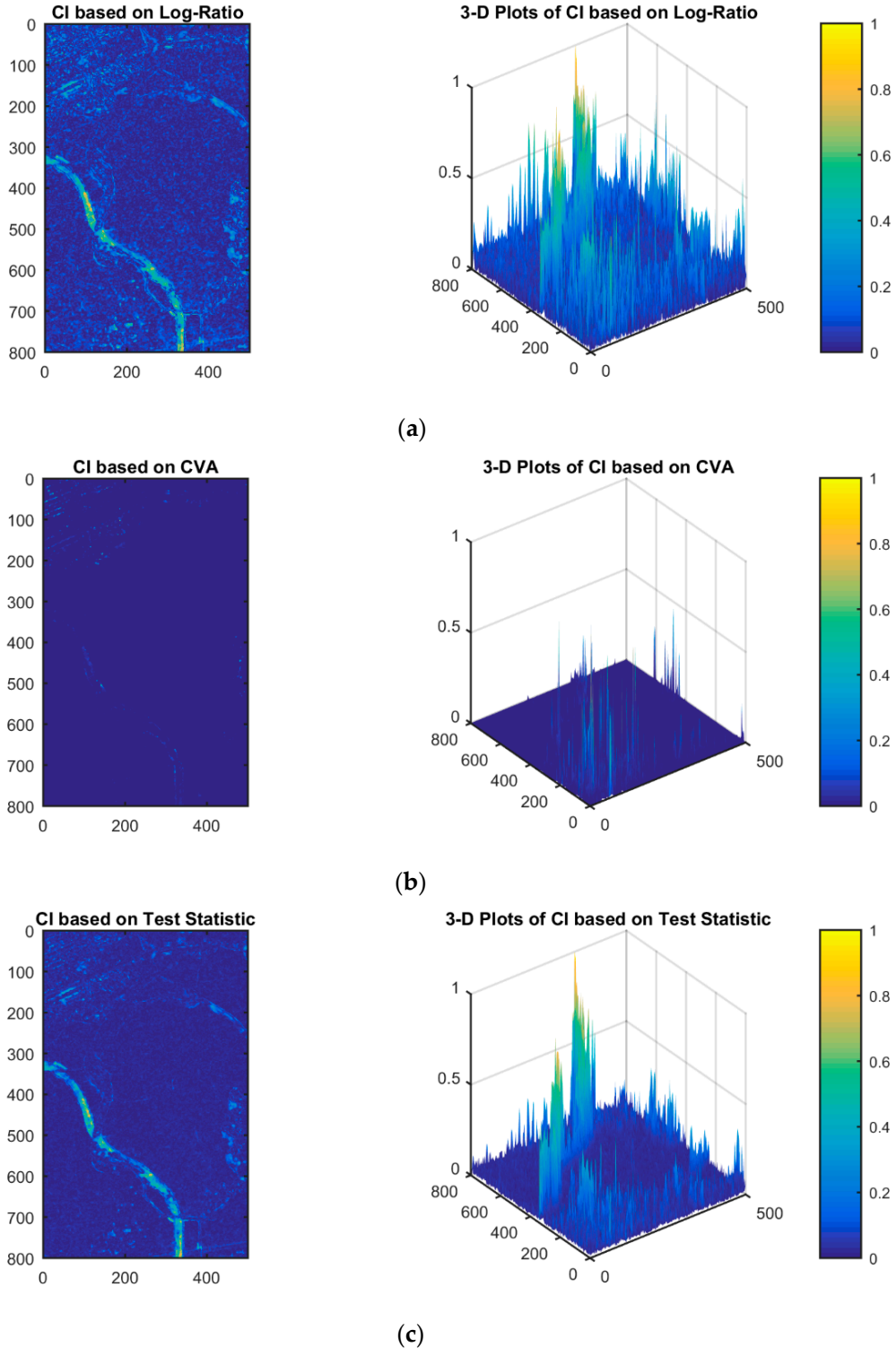

Figure 8. CI maps and 3-D plots of Region 1 based on (**a**) log-ratio (HH), (**b**) CVA, and (**c**) test statistics for the different dates of 25 June 2015 and 6 July 2016.

After generating the CI maps, the change detection maps were obtained by the threshold methods of a 5% significance level, a 1% significance level, K&I, CFAR (Pfa = 0.005), and a test statistic and improved K&I (the proposed method). The results are shown in Figures 9 and 10, where it can be seen that the obvious changed areas can be easily detected by all methods. In order to further verify the efficiency of the proposed method in generating the CI, we used the same threshold strategy

(improved K&I) in the methods of log-ratio of single-channel SAR, CVA, and test statistics, as shown in Figure 9a–d,i and Figure 10a–d,i. As a result of the effect of speckle noise and the CI map with lower contrast, the results of log-ratio and improved K&I based on single-channel bi-temporal SAR images contain many wrong detections in some unchanged areas. The other change detection method of CVA and improved K&I results in many missed detections. Due to the high quality of the CI map obtained using the fully polarimetric information based on the test statistic, the change detection map of the test statistic and improved K&I shows a better performance. These experiments show that using the multi-temporal full polarimetric data can achieve a better change detection result than using single-channel or multi-channel data. In order to compare the effect of the threshold choice, we used the CI map based on the test statistic and the threshold methods of 5% significance level, 1% significance level, K&I, CFAR (Pfa = 0.005), and improved K&I. Among these methods of choosing the threshold, 5% and 1% significance levels and K&I result in more false alarms in the region of city and forest than improved K&I. In addition, CFAR results in more false alarms in the region of water bodies than the proposed method. The quantitative comparisons of these detection schemes shown in Tables 1 and 2 also indicate that the proposed approach shows a better performance. The proposed approach of the test statistic and improved K&I achieves the best results in all four indicators (FA (%), TE (%), OA (%), and Kappa). This confirms that the proposed method is effective and shows a significant improvement over the other methods.

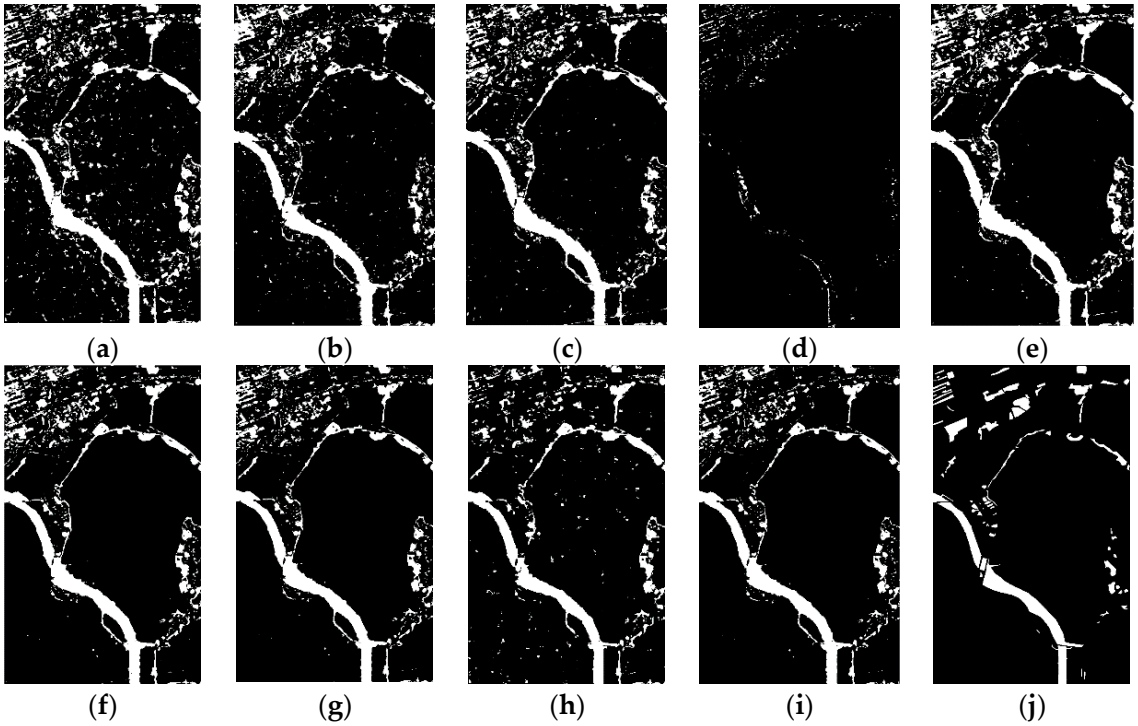

Figure 9. Change detection results in Region 1 between 7 December 2011 and 25 June 2015 based on the following: (**a**) log-ratio (HH) and improved K&I; (**b**) log-ratio (HV) and improved K&I; (**c**) log-ratio (VV) and improved K&I; (**d**) CVA and improved K&I; (**e**) test statistic with 5% significance level; (**f**) test statistic with 1% significance level; (**g**) test statistic and K&I; (**h**) test statistic and CFAR; (**i**) test statistic and improved K&I (the proposed method); (**j**) Ground reference (white denotes the change and black denotes the non-change).

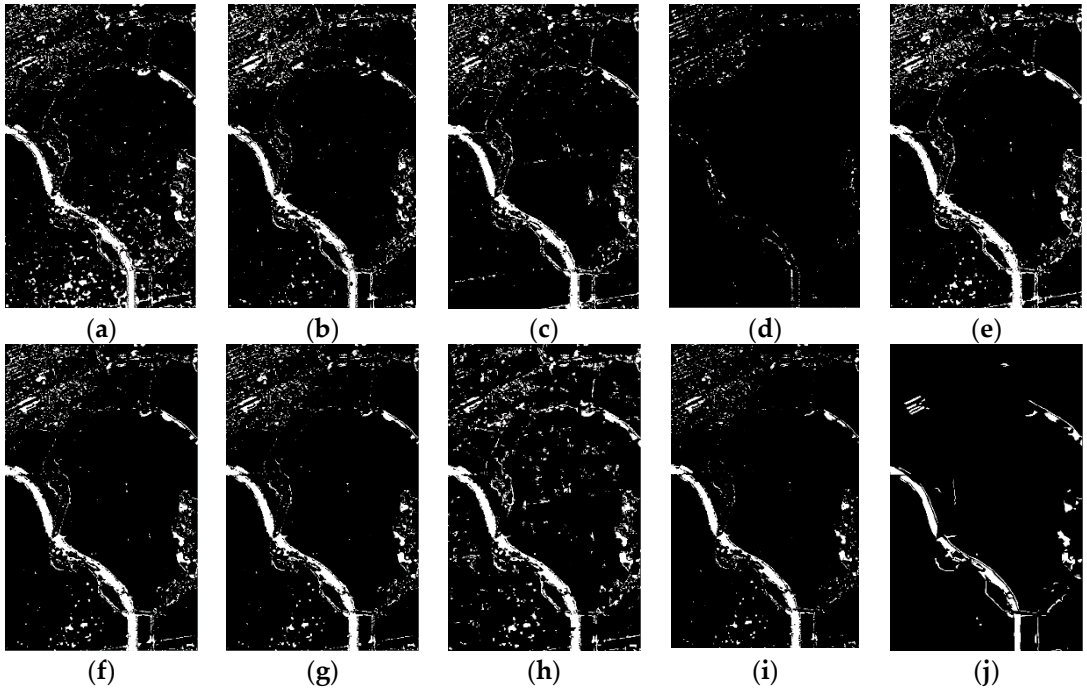

Figure 10. Change detection results in Region 1 between 25 June 2015 and 6 July 2016 based on the following: (**a**) log-ratio (HH) and improved K&I; (**b**) log-ratio (HV) and improved K&I; (**c**) log-ratio (VV) and improved K&I; (**d**) CVA and improved K&I; (**e**) test statistic with 5% significance level; (**f**) test statistic with 1% significance level; (**g**) test statistic and K&I; (**h**) test statistic and CFAR; (**i**) test statistic and improved K&I (the proposed method); (**j**) Ground reference (white denotes the change and black denotes the non-change).

Table 1. Performance evaluation of the change detection on East Lake between 2011 and 2015.

Method	FA (%)	TE (%)	OA (%)	KAPPA
HH and improved K&I	10.49	11.17	88.83	0.4574
HV and improved K&I	7.78	8.67	91.33	0.5292
VV and improved K&I	8.45	9.31	90.69	0.5078
CVA and improved K&I	0.67	7.41	92.59	0.0994
Test statistic with 5% significance level	8.77	9.32	90.68	0.5204
Test statistic with 1% significance level	6.9	7.82	92.18	0.5597
Test statistic and K&I	6.16	7.24	92.76	0.5757
Test statistic and CFAR	5.99	7.32	92.68	0.5626
Test statistic and improved K&I (the proposed method)	5.79	6.98	93.02	0.5827

Table 2. Performance evaluation of the change detection on East Lake between 2015 and 2016.

Method	FA (%)	TE (%)	OA (%)	KAPPA
HH and improved K&I	6.55	7.03	92.96	0.4413
HV and improved K&I	5.06	5.80	94.20	0.4774
VV and improved K&I	5.19	5.67	94.33	0.5041
CVA and improved K&I	1.03	4.73	95.27	0.0415
Test statistic with 5% significance level	6.17	6.42	93.58	0.4857
Test statistic with 1% significance level	4.59	5.04	94.96	0.5398
Test statistic and K&I	3.96	4.51	95.49	0.5629
Test statistic and CFAR	6.53	6.84	93.16	0.4630
Test statistic and improved K&I (the proposed method)	2.69	3.51	96.49	0.6098

3.1.2. Change Detection Based on the 2015 and 2016 Images

The highlighted box labeled as Region 2 (Yanxi Lake) is used to give a detailed assessment. This region contains grassland, city, and water bodies, and the size is 800 × 500 pixels. The main changes occurred in the water areas and the city. The RGB images in Pauli basis ($|S_{hh} - S_{vv}|$ for red, $|S_{hv}|$ for green, and $|S_{hh} + S_{vv}|$ for blue) and the ground reference of the changed areas are shown in Figure 11.

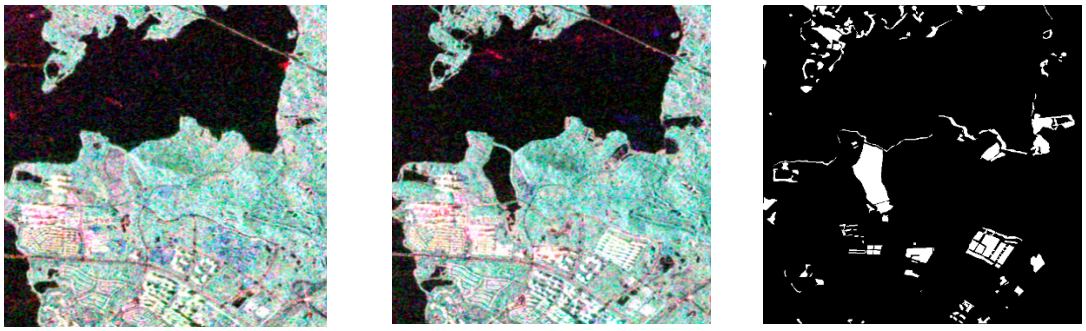

(**a**) (**b**) (**c**)

Figure 11. RADARSAT-2 PolSAR images of Region 2 indicated in Figure 3, acquired on (**a**) 25 June 2015 and (**b**) 6 July 2016; (**c**) The ground reference map (white denotes change and black denotes non-change).

The results of the CI maps and their 3-D plots are shown by linear mapping to [0, 1] in Figure 12. Although the CI map of the log-ratio (HH) method (Figure 12a) shows a strong response in the changed area, the contrast between the changed and unchanged areas is not obvious. Moreover, there is also a high response in the unchanged area because of the speckle noise, which impacts the accuracy of the change detection map. The CI map of the CVA method (Figure 12b) shows a weak response, which makes it difficult to distinguish the changed and unchanged areas. The proposed method (Figure 12c) using the fully polarimetric information also shows a strong response in the changed areas. However, unlike the other methods, the CI values are almost homogeneous in the water bodies and forest areas. Overall, the proposed method of generating the CI map is effective at accurately distinguishing the changed and unchanged areas.

After generating the CI maps, the change detection maps were obtained by the threshold methods of 5% significance level, 1% significance level, K&I, CFAR (Pfa = 0.005), and the proposed method. The results are shown in Figure 13, where it can be seen that the obviously changed areas can be easily detected by all the methods. In order to further verify the efficiency of the proposed method in generating the CI map, we used the same threshold strategy (improved K&I) in the methods of log-ratio of single-channel SAR, CVA, and test statistics, as shown in Figure 13a–d,i. As a result of the speckle noise and the CI map with lower contrast, the result of log-ratio and improved K&I based on single-channel bi-temporal SAR images contains many wrong detections in some unchanged areas. The other change detection method of CVA and improved K&I results in many missed detections. Due to the high quality of the CI map obtained using the fully polarimetric information based on the test statistic, the change detection map of the test statistic and improved K&I shows a better performance. These experiments show that using the multi-temporal full polarimetric data can achieve a better change detection result than using the single-channel or multi-channel data. In order to compare the effect of the threshold choice, we used the CI map based on the test statistic and the threshold methods of 5% significance level, 1% significance level, K&I, CFAR (Pfa = 0.005), and improved K&I. Among these methods of choosing the threshold, the 5% and 1% significance levels and K&I result in more false alarms in the city and forest than the proposed method. In addition, CFAR results in more false alarms in the water bodies than the proposed method. The quantitative comparison of these detection schemes shown in Table 3 also indicates that the proposed approach shows a better performance. The proposed approach of the test statistic and improved K&I achieves the best results

in all four indicators (FA (%), TE (%), OA (%), and Kappa). This confirms that the proposed method is effective and shows a significant improvement over the other methods.

The image of Yandong Lake (400 × 400 pixels) contains grassland, city, and water bodies. The main changes occurred in the water areas, because of the rain. The RGB images in Pauli basis ($|S_{hh} - S_{vv}|$ for red, $|S_{hv}|$ for green, and $|S_{hh} + S_{vv}|$ for blue), and the reference data of the changed areas are shown in Figure 14.

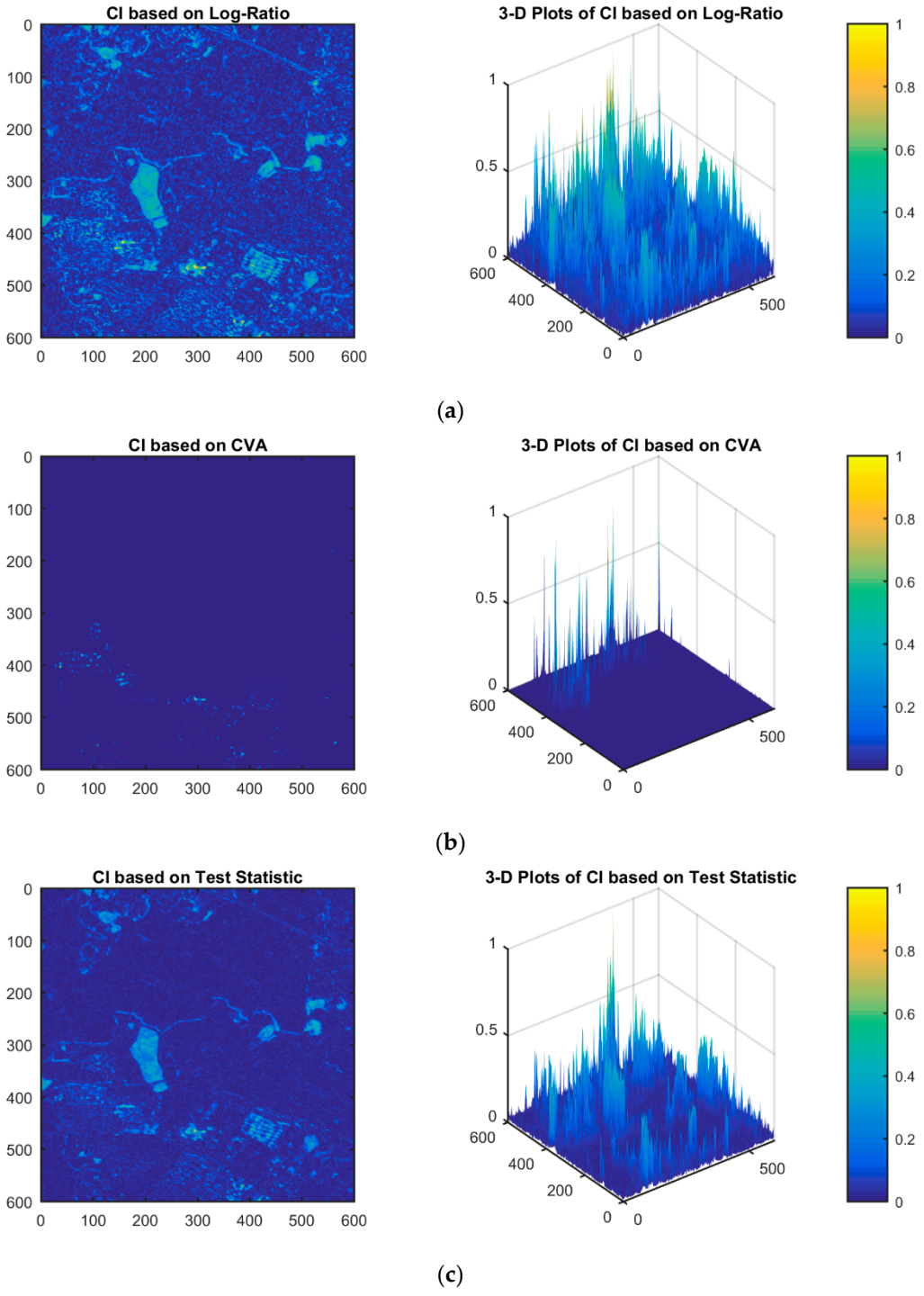

Figure 12. CI maps and 3-D plots of Region 2 based on (**a**) log-ratio, (**b**) CVA, and (**c**) test statistics at the different dates of 25 June 2015 and 6 July 2016.

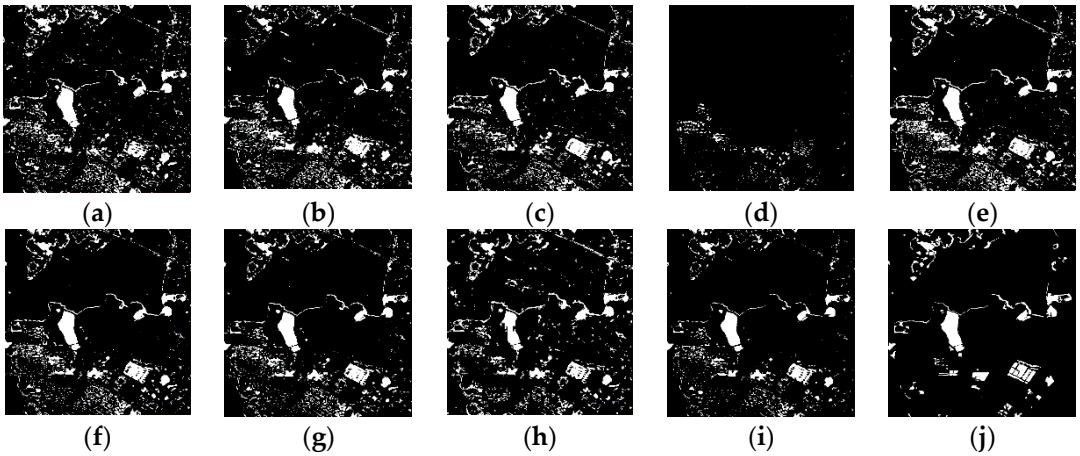

Figure 13. Change detection results in Region 2 between 25 June 2015 and 6 July 2016 based on the following: (**a**) log-ratio (HH) and improved K&I; (**b**) log-ratio (HV) and improved K&I; (**c**) log-ratio (VV) and improved K&I; (**d**) CVA and improved K&I; (**e**) test statistic with 5% significance level; (**f**) test statistic with 1% significance level; (**g**) test statistic and K&I; (**h**) test statistic and CFAR; (**i**) test statistic and improved K&I (the proposed method); (**j**) Ground reference (white denotes the change and black denotes the non-change).

Table 3. Performance evaluation of the change detection on Yanxi Lake between 2015 and 2016.

Method	FA (%)	TE (%)	OA (%)	KAPPA
HH and improved K&I	6.69	7.97	92.03	0.5135
HV and improved K&I	6.51	7.99	92.01	0.5026
VV and improved K&I	6.37	7.50	92.50	0.5388
CVA and improved K&I	1.08	7.36	92.64	0.0599
Test statistic with 5% significance level	7.22	7.99	92.01	0.5358
Test statistic with 1% significance level	5.37	6.57	93.43	0.5749
Test statistic and K&I	4.86	6.19	93.81	0.5862
Test statistic and CFAR	6.70	7.92	92.08	0.5179
Test statistic and improved K&I (the proposed method)	3.18	5.09	94.91	0.6141

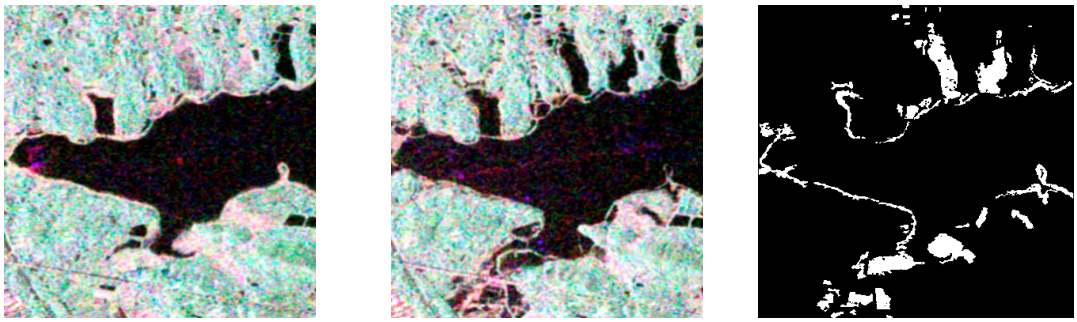

Figure 14. RADARSAT-2 PolSAR images of Region 2 indicated in Figure 3, acquired on (**a**) 25 June 2015 and (**b**) 6 July 2016. (**c**) The ground-truth map (white denotes the change and black denotes the non-change).

The results of the CI maps and their 3-D plots are shown by linear mapping to [0, 1] in Figure 15. Although the CI map of the log-ratio (HH) method (Figure 15a) shows a strong response in the water bodies, the contrast between the changed and unchanged areas is not obvious. Moreover, there is also a high response in the unchanged area because of the speckle noise, which impacts the accuracy of the

change detection map. The CI map of the CVA method (Figure 15b) shows a weak response, which makes it difficult to distinguish the changed and unchanged areas. The proposed method (Figure 15c) shows a strong response in the water bodies corresponding to the changed parts and low values in the water bodies corresponding to the unchanged parts. Overall, the proposed method of generating the CI map is effective at accurately distinguishing changed and unchanged areas.

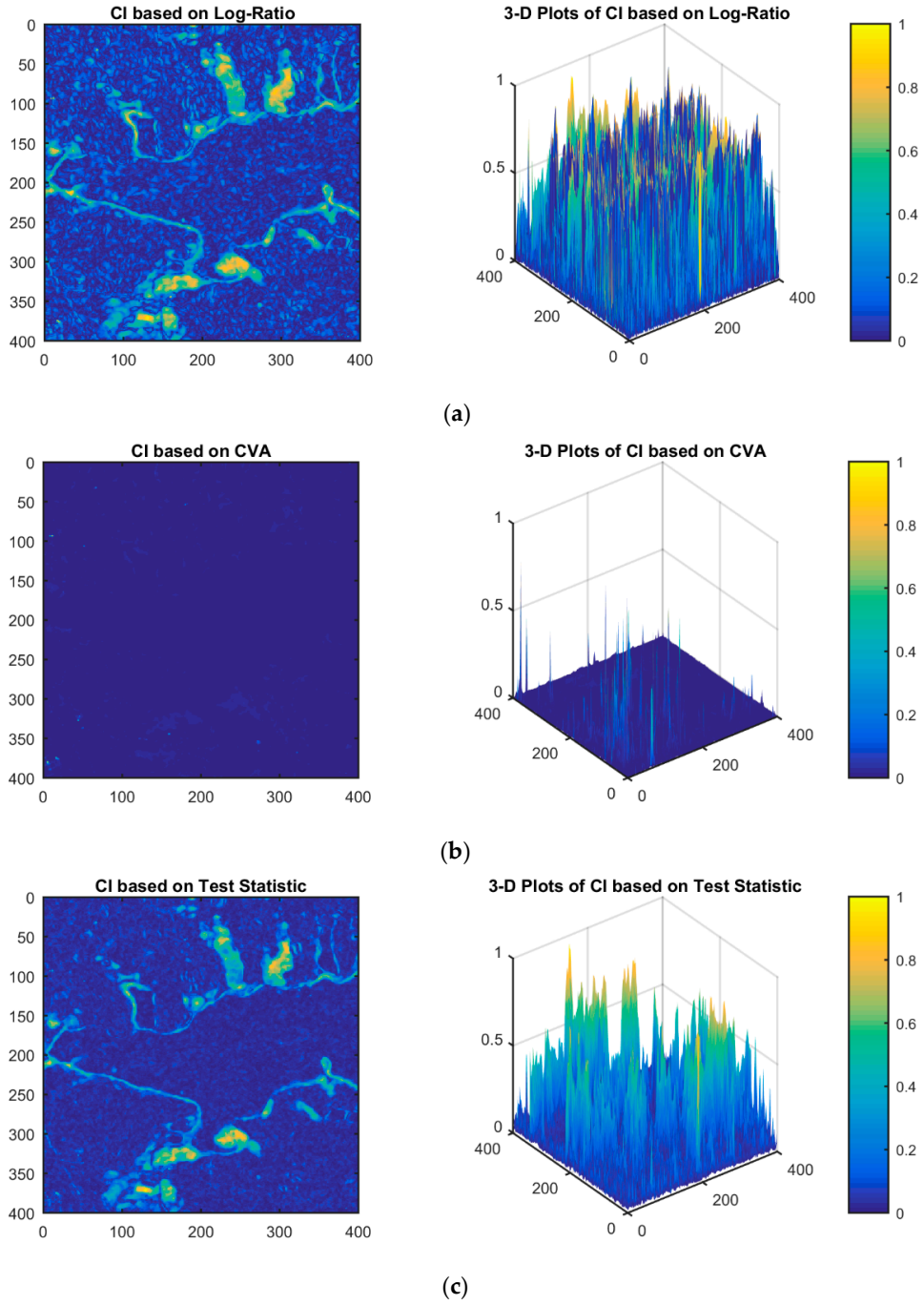

Figure 15. CI maps and 3-D plots of Region 3 based on (**a**) log-ratio, (**b**) CVA, and (**c**) test statistics at the different dates of 25 June 2015 and 6 July 2016.

After generating the CI maps, the change detection maps were obtained by the threshold methods of 5% significance level, 1% significance level, K&I, CFAR (Pfa = 0.005), and the proposed method. The results are shown in Figure 16, where it can be seen that the obviously changed areas can be

easily detected by all the methods. In order to further verify the efficiency of the proposed method in generating the CI, we used the same threshold strategy (improved K&I) in the methods of log-ratio of single-channel SAR, CVA, and test statistics, as shown in Figure 16a–d,i. As a result of the speckle noise and CI map with lower contrast, the result of log-ratio and improved K&I based on single-channel bi-temporal SAR images contains many wrong detections in some unchanged areas. The other change detection method of CVA and improved K&I results in many missed detections. Due to the high quality of the CI map obtained using the fully polarimetric information based on the test statistic, the change detection map of the test statistic and improved K&I shows a better performance. These experiments show that using the multi-temporal full polarimetric data can achieve a better change detection result than using single-channel or multi-channel data. In order to compare the effect of the threshold choice, we used the CI map based on the test statistic and the threshold methods of 5% significance level, 1% significance level, K&I, CFAR (Pfa = 0.005), and improved K&I. Among these methods of choosing the threshold, the 5% and 1% significance levels and K&I result in more false alarms in the city and forest than the proposed method. In addition, CFAR results in more false alarms in the water bodies than the proposed method. The quantitative comparison of these detection schemes shown in Table 4 also indicates that the proposed approach shows a better performance. The proposed approach of the test statistic and improved K&I achieves the best results in all four indicators (FA (%), TE (%), OA (%), Kappa). This confirms that the proposed method is effective and shows a significant improvement over the other methods.

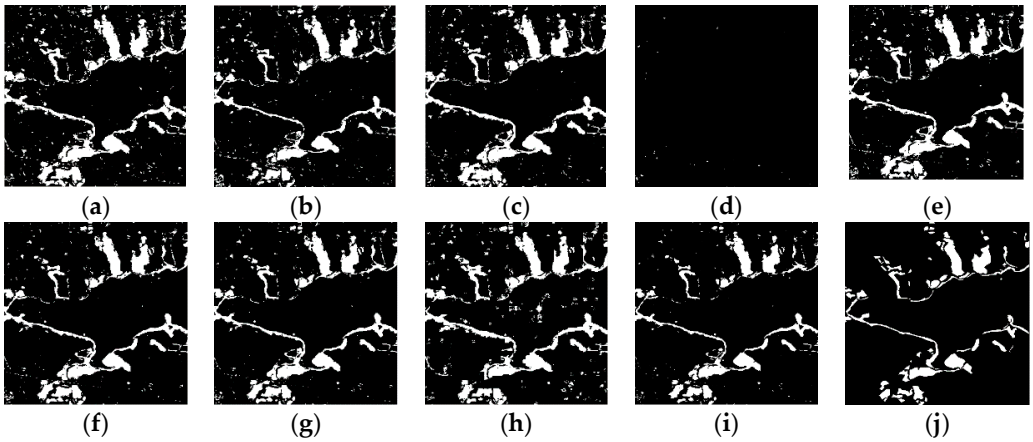

Figure 16. Change detection results in Region 3 between 25 June 2015 and 6 July 2016 based on the following: (**a**) log-ratio (HH) and improved K&I; (**b**) log-ratio (HV) and improved K&I; (**c**) log-ratio (VV) and improved K&I; (**d**) CVA and improved K&I; (**e**) test statistic with 5% significance level; (**f**) test statistic with 1% significance level; (**g**) test statistic and K&I; (**h**) test statistic and CFAR; (**i**) test statistic and improved K&I (the proposed method); (**j**) Ground reference (white denotes the change and black denotes the non-change).

Table 4. Performance evaluation of the change detection on Yandong Lake between 2015 and 2016.

Method	FA (%)	TE (%)	OA (%)	KAPPA
HH and improved K&I	7.15	7.62	92.38	0.6402
HV and improved K&I	4.78	6.23	93.77	0.6686
VV and improved K&I	6.53	7.15	92.85	0.6541
CVA and improved K&I	0.09	9.35	90.65	0.0017
Test statistic with 5% significance level	6.80	7.17	92.83	0.6593
Test statistic with 1% significance level	5.30	6.09	93.91	0.6906
Test statistic and K&I	5.64	5.92	94.08	0.6755
Test statistic and CFAR	7.67	8.28	91.72	0.6130
Test statistic and improved K&I (the proposed method)	3.26	4.81	95.19	0.7282

4. Conclusions

In this paper, we have presented an improved multi-temporal PolSAR image change detection approach. A test statistic based on MLE and improved K&I were used to deal with the problem of change detection of a complex urban area containing bridges, water bodies, and buildings. Multi-temporal data of Wuhan, China, were used to assess the performance of the proposed method. The main advantages of the proposed method are (1) the use of fully polarimetric information, (2) the use of the GGM to choose the PolSAR threshold, and (3) the computational simplicity and stability. Because obtaining the CI map is the key step in unsupervised change detection, the log-ratio method using single-channel information and CVA using linear computation of multi-channel information cannot generate a high-quality CI map, which directly influences the precision of the change detection map. The proposed method using fully polarimetric information is better able to detect slight differences and can effectively distinguish between changed and unchanged areas. The use of a test statistic is appropriate for PolSAR images, and it can be used to obtain an accurate CI map. The use of K&I to automatically choose the threshold under the assumption that the PDF of the CI follows a Gaussian distribution does not accurately match the aforementioned conditional densities of classes. We therefore use the improved K&I algorithm based on the GGM to choose the threshold. Using the proposed method, we were able to accurately detect the changes associated with the construction of a tunnel on East Lake from 2011 to 2016, as well as the changes in water bodies caused by the heavy rainfall in July 2016. The experimental results obtained on the multi-temporal PolSAR images of Wuhan confirmed the effectiveness of the proposed approach.

Acknowledgments: The authors would like to thank the National Natural Science Foundation of China (grant no. 91438203, no. 61371199, no. 41501382, no. 41601355), the Public Welfare Project of Surveying and Mapping Interest (201412002), the Hubei Provincial Natural Science Foundation (no. 2015CFB328, no. 2016CFB246), the National Basic Technology Program of Surveying and Mapping (no. 2016KJ0103), and the Technology of Target Recognition Based on GF-3 Program (no. 03-Y20A10-9001-15/16). Jinqi Zhao would also like to thank China Scholarship Council for funding his study at Southern Methodist University.

Author Contributions: Jinqi Zhao defined the research problem, proposed the method, undertook most of the programming in MATLAB and VS2010, and wrote the paper. Jie Yang gave some key advice. Zhong Lu gave useful advice and contributed to the paper writing. Pingxiang Li provided the RADARSAT-2 data and some useful advice. Wensong Liu collected the data and processed the datasets in ENVI, PolSARpro, and NEST software. Le Yang obtained the ground-truth map.

Conflicts of Interest: The authors declare no conflict of interest.

References

1. Singh, A. Review article digital change detection techniques using remotely-sensed data. *Int. J. Remote Sens.* **1989**, *10*, 989–1003. [CrossRef]
2. Bruzzone, L.; Bovolo, F. A novel framework for the design of change-detection systems for very-high-resolution Remote Sensing Images. *Proc. IEEE* **2013**, *101*, 609–630. [CrossRef]
3. Anaya, J.A.; Colditz, R.R.; Valencia, G.M. Land Cover Mapping of a Tropical Region by Integrating Multi-Year Data into an Annual Time Series. *Remote Sens.* **2015**, *7*, 16274–16292. [CrossRef]
4. Zhao, J.Q.; Yang, J.; Li, P.X.; Liu, M.Y.; Shi, Y.M. An Unsupervised Change Detection Based on Test Statistic and KI from Multi-temporal and Full Polarimetric SAR Images. *Int. Arch. Photogramm. Remote Sens. Spat. Inf. Sci.* **2016**, *XLI-B7*, 611–615. [CrossRef]
5. Conradsen, K.; Nielsen, A.A.; Sehou, J.; Skriver, H. A test statistic in the complex Wishart distribution and its application to change detection in polarimetric SAR data. *IEEE Trans. Geosci. Remote Sens.* **2003**, *41*, 4–19. [CrossRef]
6. Zhao, L.; Yang, J.; Li, P.; Zhang, L. Seasonal inundation monitoring and vegetation pattern mapping of the Erguna floodplain by means of a RADARSAT-2 fully polarimetric time series. *Remote Sens. Environ.* **2014**, *152*, 426–440. [CrossRef]
7. Celik, T. Unsupervised change detection in satellite images using principal component analysis and k-means clustering. *IEEE Geosci. Remote Sens. Lett.* **2009**, *6*, 772–776. [CrossRef]

8. Lu, Z.; Kwoun, O.-I. Radarsat-1 and ERS InSAR analysis over southeastern coastal Louisiana: Implications for mapping water-level changes beneath swamp forests. *IEEE Trans. Geosci. Remote Sens.* **2008**, *46*, 2167–2184. [CrossRef]
9. Akbari, V.; Anfinsen, S.N.; Doulgeris, A.P.; Eltoft, T.; Moser, G.; Serpico, S.B. Polarimetric SAR Change Detection With the Complex Hotelling—Lawley Trace Statistic. *IEEE Trans. Geosci. Remote Sens.* **2016**, *54*, 3953–3966. [CrossRef]
10. Caves, R.; Quegan, S. Segmentation based change detection in ERS-1 SAR images. In Proceedings of the 1994 International Geoscience and Remote Sensing Symposium, IGARSS'94 Surface and Atmospheric Remote Sensing: Technologies, Data Analysis and Interpretation, New York, NY, USA, 9 December 1994; pp. 2149–2151.
11. Hachicha, S.; Chaabane, F. On the SAR change detection review and optimal decision. *Int. J. Remote Sens.* **2014**, *35*, 1693–1714. [CrossRef]
12. Bovolo, F.; Bruzzone, L. The time variable in data fusion: A change detection perspective. *IEEE Geosci. Remote Sens. Mag.* **2015**, *3*, 8–26. [CrossRef]
13. Rignot, E.J.; van Zyl, J.J. Change detection techniques for ERS-1 SAR data. *IEEE Trans. Geosci. Remote Sens.* **1993**, *31*, 896–906. [CrossRef]
14. Bazi, Y.; Bruzzone, L.; Melgani, F. An unsupervised approach based on the generalized Gaussian model to automatic change detection in multitemporal SAR images. *IEEE Trans. Geosci. Remote Sens.* **2005**, *43*, 874–887. [CrossRef]
15. Moser, G.; Serpico, S.B. Generalized minimum-error thresholding for unsupervised change detection from SAR amplitude imagery. *IEEE Trans. Geosci. Remote Sens.* **2006**, *44*, 2972–2982. [CrossRef]
16. Sumaiya, M.; Kumari, R.S.S. Logarithmic Mean-Based Thresholding for SAR Image Change Detection. *IEEE Geosci. Remote Sens. Lett.* **2016**, *13*, 1726–1728. [CrossRef]
17. Liu, M.; Zhang, H.; Wang, C.; Wu, F. Change detection of multilook polarimetric SAR images using heterogeneous clutter models. *IEEE Trans. Geosci. Remote Sens.* **2014**, *52*, 7483–7494.
18. Zhao, J.; Yang, J.; Lu, Z.; Li, P.; Liu, W.; Yang, L. A Novel Method of Change Detection in Bi-Temporal PolSAR Data Using a Joint—Classification Classifier Based on a Similarity Measure. *Remote Sens.* **2017**, *9*, 846. [CrossRef]
19. Liu, W.; Yang, J.; Zhao, J.; Yang, L. A Novel Method of Unsupervised Change Detection Using Multi-Temporal PolSAR Images. *Remote Sens.* **2017**, *9*, 1135. [CrossRef]
20. Brown, L.G. A survey of image registration techniques. *ACM Comput. Surv. (CSUR)* **1992**, *24*, 325–376. [CrossRef]
21. Inglada, J.; Giros, A. On the possibility of automatic multisensor image registration. *IEEE Trans. Geosci. Remote Sens.* **2004**, *42*, 2104–2120. [CrossRef]
22. Lee, J.-S.; Pottier, E. *Polarimetric Radar Imaging: From Basics to Applications*; CRC Press: Boca Raton, FL, USA, 2009.
23. Alberga, V. Similarity measures of remotely sensed multi-sensor images for change detection applications. *Remote Sens.* **2009**, *1*, 122–143. [CrossRef]
24. Alonso-González, A.; López-Martínez, C.; Salembier, P. PolSAR time series processing with binary partition trees. *IEEE Trans. Geosci. Remote Sens.* **2014**, *52*, 3553–3567. [CrossRef]
25. Lang, F.; Yang, J.; Li, D.; Zhao, L.; Shi, L. Polarimetric SAR image segmentation using statistical region merging. *IEEE Geosci. Remote Sens. Lett.* **2014**, *11*, 509–513. [CrossRef]
26. Yang, W.; Yang, X.; Yan, T.; Song, H.; Xia, G.-S. Region-Based Change Detection for Polarimetric SAR Images Using Wishart Mixture Models. *IEEE Trans. Geosci. Remote Sens.* **2016**, *54*, 6746–6756. [CrossRef]
27. Lu, D.; Mausel, P.; Brondizio, E.; Moran, E. Change detection techniques. *Int. J. Remote Sens.* **2004**, *25*, 2365–2401. [CrossRef]
28. Qiu, B.; Prinet, V.; Perrier, E.; Monga, O. Multi-block PCA method for image change detection. In Proceedings of the 2003 12th International Conference on Image Analysis and Processing, Mantova, Italy, 17–19 September 2003; pp. 385–390.
29. Yousif, O.; Ban, Y. Improving urban change detection from multitemporal SAR images using PCA-NLM. *IEEE Trans. Geosci. Remote Sens.* **2013**, *51*, 2032–2041. [CrossRef]
30. Carincotte, C.; Derrode, S.; Bourennane, S. Unsupervised change detection on SAR images using fuzzy hidden Markov chains. *IEEE Trans. Geosci. Remote Sens.* **2006**, *44*, 432–441. [CrossRef]

31. Bouyahia, Z.; Benyoussef, L.; Derrode, S. Change detection in synthetic aperture radar images with a sliding hidden Markov chain model. *J. Appl. Remote Sens.* **2008**, *2*, 023526.
32. Inglada, J.; Mercier, G. A new statistical similarity measure for change detection in multitemporal SAR images and its extension to multiscale change analysis. *IEEE Trans. Geosci. Remote Sens.* **2007**, *45*, 1432–1445. [CrossRef]
33. Gao, G.; Liu, L.; Zhao, L.; Shi, G.; Kuang, G. An adaptive and fast CFAR algorithm based on automatic censoring for target detection in high-resolution SAR images. *IEEE Trans. Geosci. Remote Sens.* **2009**, *47*, 1685–1697. [CrossRef]
34. Jung, C.H.; Song, W.Y.; Rho, S.H.; Kim, J.; Park, J.T.; Kwag, Y.K. Double-step fast CFAR scheme for multiple target detection in high resolution SAR images. In Proceedings of the 2010 IEEE Radar Conference, Washington, DC, USA, 10–14 May 2010; pp. 1172–1175.
35. Otsu, N. A threshold selection method from gray-level histograms. *Automatica* **1975**, *11*, 23–27. [CrossRef]
36. Kapur, J.N.; Sahoo, P.K.; Wong, A.K. A new method for gray-level picture thresholding using the entropy of the histogram. *Comput. Vis. Graph. Image Process.* **1985**, *29*, 273–285. [CrossRef]
37. Kittler, J.; Illingworth, J. Minimum error thresholding. *Pattern Recognit.* **1986**, *19*, 41–47. [CrossRef]
38. Sharifi, K.; Leon-Garcia, A. Estimation of shape parameter for generalized Gaussian distributions in subband decompositions of video. *IEEE Trans. Circuits Syst. Video Technol.* **1995**, *5*, 52–56. [CrossRef]
39. Lee, J.S.; Jurkevich, L.; Dewaele, P.; Wambacq, P.; Oosterlinck, A. Speckle filtering of synthetic aperture radar images: A review. *Remote Sens. Rev.* **1994**, *8*, 313–340. [CrossRef]
40. Pham, M.T.; Mercier, G.; Michel, J. Change detection between SAR images using a pointwise approach and graph theory. *IEEE Trans. Geosci. Remote Sens.* **2016**, *54*, 2020–2032. [CrossRef]
41. Stehman, S.V. Selecting and interpreting measures of thematic classification accuracy. *Remote Sens. Environ.* **1997**, *62*, 77–89. [CrossRef]